Article:
Dorgham, A, Azam, A orcid.org/0000-0002-3510-1333, Parsaeian, P et al. (3 more authors) (2021) Nanoscale viscosity of triboreactive interfaces. Nano Energy, 79. 105447. ISSN 2211-2855

https://doi.org/10.1016/j.nanoen.2020.105447

Nanoscale viscosity of triboreactive interfaces

Abdel Dorgham[†,*], Abdullah Azam[†], Pourya Parsaeian[†], Chun Wang[†], Ardian Morina[†], and Anne Neville[†]

[†]Institute of Functional Surfaces, School of Mechanical Engineering, University of Leeds, Leeds LS2 9JT, UK
[*]Corresponding author: a.dorgham@leeds.ac.uk

ABSTRACT

It has been long speculated that the good antiwear properties of the nano-thin triboreactive interfaces might have a rheological origin that can greatly influence their friction, lubrication and antiwear characteristics, which account for nearly one quarter of the worldwide total energy consumption. However, the measurement of the nanoscale viscosity of such tribological interfaces is still a challenging task. This is mainly due to their ultralow thickness, i.e. typically < 150 nm, high viscosity and reactivity, which make the currently used bulk, interfacial or micro-gap rheological techniques inadequate. Here we demonstrate two methods, i.e. creep and squeeze flow, that can be used to quantify the viscosity of triboreactive films in-situ as they form and ex-situ after formation. Films generated from the zinc and ashless dialkyldithiophosphate (ZDDP and DDP) antiwear additives were analysed as model systems because of their industrial and academic importance. The results confirm that the formed tribofilms behave as molten glass with an average viscosity ranging from 2×10^{11} to 7×10^{12} Pa.s. During its formation, the molten glass showed rich intrinsic rheological properties that allowed them to maintain local order on the nanoscale through the motion and reconfiguration of single and multiple patches within the formed film, which can significantly predetermine its superior antiwear properties. The findings of this study open future opportunities for optimising the nano-flowable glass to efficiently control the lubrication of tomorrow's engines without the need of any environmentally harmful oil additives.

Keywords: nanoscale viscosity, rheology, creep, squeeze flow, tribology, ZDDP tribofilm

1 Introduction

A massive proportion, about one quarter, of the world's total energy is consumed within tribological contacts, rubbing against each other, to partly overcome friction or due to wear[1,2]. Worldwide, proactive measures, for instance by reducing friction and wear, can save more than 1.39% in the Gross National Product (GNP) and more than 8.7% of the total fuel energy consumption within the next 15 years[2]. The use of antiwear additives in lubricating oils is one of the proactive measures to reduce wear and thus avoid considerable energy losses. Triboreactive films formed from P-based oil additives such as ZDDP and DDP attract considerable attention for their superior, yet not fully elucidated, antiwear capability. The generation of these triboreactive films in lubricating oils is a complex multistage process[3,4]. It all starts with rubbing, which occurs between contacting surfaces such as in the cylinder/piston geometry in a typical internal combustion engine (ICE), as demonstrated in Figure 1. Due to rubbing at high temperature, the molecules of ZDDP additive ($Zn[(RO)_2PS_2]_2$) in the lubricating oil start to self- and trans-alkylate (Figure 1b), which involves the migration of alkyl groups from the O to S atoms[5–7]. The additive then adsorbs to the steel substrate as either unreacted molecules or as linkage isomers ($Zn[O_2P\ (SR)_2]_2$)[8]. In the case of rubbing the countersurfaces at high temperature and contact pressure, two phenomena are greatly accelerated. First, iron cations are released from the steel substrate[9]. Second, the adsorbed ZDDP molecules undergo a partial decomposition into zinc and iron sulphate followed by their reduction into sulphide species[7,10]. Heat causes sulphur to diffuse into the steel[11], whereas shear and rubbing assist the formation of a mixed oxide-sulphide base layer of isolated clusters[12,13] (Figure 1c). The base layer acts as a glue providing excellent tenacity between the steel surface and the subsequently formed layers of amorphous iron and zinc polyphosphate chains of increasing length towards the film's surface[12,14] (Figure 1d). These layers mark the final decomposition stage of the ZDDP molecules.

The resulting amorphous polyphosphate forms a unique antiwear structure of growing thickness and patchiness as sliding cycles increase (Figure 1e). The antiwear protection of such an evolving structure has been attributed to its rigid sacrificial nature[15,16] and its ability to digest the sharp worn particles[17,18]. These mechanisms are either mechanical or chemical in nature. However, few studies[9,12,19–21] speculated that the good antiwear properties might have a rheological origin, which can greatly influence friction, lubrication and adhesion properties of any tribological surface[22]. For instance, it was suggested[9,12,19] that the layers close to the metal surface, e.g. zinc/iron sulphides and phosphates, are most likely elastic or elastoplastic solids that can be polymeric in nature[20], whereas the outer layers are viscous. This indicates that there can be layers in between that have a combination of the two and thus contribute differentially to the overall behaviour of the film[9]. The top viscous layer can explain

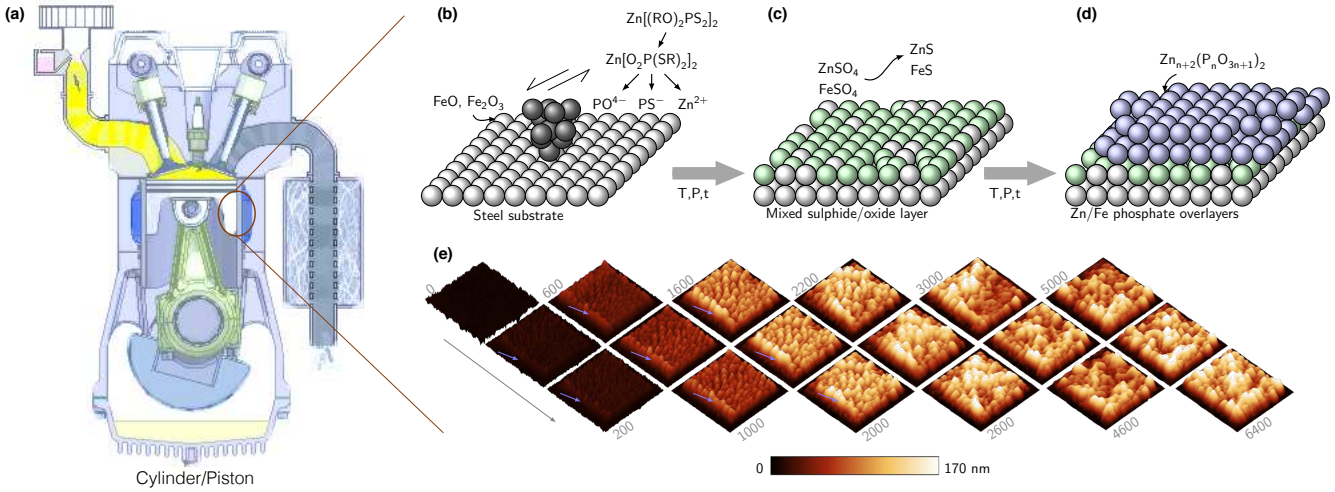

Figure 1. Ultrathin ZDDP triboreactive films. a, Schematic illustration of a cylinder/piston geometry inside a typical ICE, b, c, and d, ZDDP tribofilm formation at high temperature and contact pressure on the rubbing surfaces of the cylinder and piston, b, Adsorption of ZDDP additive, c, Formation of mixed oxide-sulphide base layer on the steel substrate. d, Formation of iron and zinc polyphosphate on the sulphur-oxide base layer. e, In-situ evolution of the structure of the ZDDP film formed at 80 °C and 7.3 GPa. Small arrows indicate areas of large thickness that appear initially on the side of the films. All AFM images are $6 \times 6\,\mu m^2$ in area.

the patchy pad-like structure of the film (Figure 1e) as a final solidified image of the once hot flowing glass. The ridges of this glass are formed due to asperity-asperity contact, whereas the troughs originate from possibly the flow of some material from the regions of ridges to troughs[12,23]. Other theories suggested that the pad-like structure is formed due to local variations in contact pressure[24] or surface heterogeneity[15]. However, some previous reports[3,12,18] showed that the film is also heterogeneous vertically over its depth, which indicates that the heterogeneity of the film is not solely due to local lateral variations in contact pressure[25].

Several previous studies[26–33] demonstrated various methods to measure the rheological response, i.e. mainly relaxation time, of ultrathin polymeric films. However, these methods are mainly applicable to interfaces of relatively low viscosity or above the glass transition temperature (T_g). Here, we report two methods based on creep and squeeze flow measurements that revolutionize the quantification of the rheological properties, i.e. viscosity, of highly viscous ultrathin triboreactive films. In order to observe the flowability and interaction of the different patches composing such films, in-situ AFM experiments, following the in-situ single asperity methodology proposed by Gosvami et al.[15], are used to generate pads of close and far apart local occupancy. The dynamic behaviour of these pads under shear is then analysed to deduce the viscosity of the formed films.

2 Experimental

2.1 Materials

The oil used in this study was a poly-α-olefin (PAO) base oil of a 4 cSt kinematic viscosity at 100 °C. A Secondary ZDDP and a neutral DDP antiwear additives (Figure S1) were mixed with the oil such that the concentration of P in the oil was fixed at 800 ppm. The oil and additives were supplied by Afton Chemicals (UK) and were used as received. The tribological sample was a disc made of AISI 52100 bearing steel of average Rq roughness < 13 nm.

2.2 High temperature AFM liquid cell

The AFM cell (Figure S2) consisted of an aluminium body where the sample under study, i.e. AISI 52100 bearing steel disc, can be fixed using a screw in the centre. This was sufficient to fix the sample and avoid any drift due to the high contact pressures used during the in-situ tests. The liquid cell itself was mounted on the AFM stage using four magnets. The cell was heated using two cartridge heaters (Watlow, UK), which were inserted inside at a distance 3 cm apart. The two heaters were needed in order to avoid any microflow due to thermal variations within the oil. This effect was also minimized by limiting the oil volume to less than 3 ml by reducing the size of the liquid cell. The temperature of the cartridge heaters were controlled using a PID controller (Watlow, UK) through a closed loop algorithm with two thermocouples integrated in the heaters. Furthermore, one external thermometer was used frequently to externally monitor the temperature of the oil.

2.3 In-situ atomic force microscopy

The setup used for performing the in-situ AFM tests consisted of a Dimension Icon Bruker AFM equipped with the in-house developed liquid cell. The tests were performed using standard Rtespa 300 AFM tips (Bruker, USA), which are made of antimony (n) doped Si and have a three-sided pyramid shape with a nominal height of 12 μm and nominal radius of 8 nm (Figures S3 and S4). The AFM cantilever was made of the same material as its tip and was rectangular in shape with length, width and thickness of $125 \times 40 \times 3.4$ μm, respectively. An additional layer of 40 nm of reflective aluminium was on the backside of the cantilever in order to enhance the laser signal. The cantilever had a nominal spring constant of 40 N/m and a resonant frequency of 300 kHz. The data were collected using Nanoscope v9 software (Bruker, USA). Data analysis was performed using Gwyddion v2.47 open source software.

Before starting the tribological tests, the tip was worn away at contact force 100 nN to a radius of about 75 nm after which the radius reached steady-state (Figure S4). The size of the tip was quantified using the scanning electron microscope (SEM) (Figure S3) and AFM using tip reconstruction method[34] (Figure S4) and by generating tribofilms under the AFM, where the width of the formed tribofilms reflected the effective diameter of the tip (Figures S5 and S6).

The in-situ tests were performed in a standard contact mode while the tip and sample were completely submersed in oil at 80 ^{o}C. At this temperature, thermal drift of the AFM was found to be less than 20 nm over 6 hours scanning time (Figure S7). The AFM contact mode operated a multi-pass two-directional raster scanning of different number of lines, i.e. 128, 64, 32, 16, 8, 4 and 1 lines (Figures S8 and S9). The large number of scanning lines, i.e. 128, 64 and 32, resulted in the formation of tribofilms with 'congested' morphology as the scanning lines overlap, whereas the small number of scanning lines results in a nano-structured tribofilm with distinctive lines. The number of sliding cycles varied from one test to another, but the exact values were reported in the presented results. The rubbing speed of the AFM during the in-situ tests was fixed at 400 μm/s scanning an area of 5×5 μm^2. The tribotests were interrupted regularly, i.e. once every 100 to 1000 cycles, to capture high quality AFM images of an area of 10×10 μm^2, which was centred around the rubbed area. These were capture at low contact force < 100 nN, and speed of 40 μm/s. The scanning angle throughout the tribotests and imaging was fixed at 90^{o}, i.e. perpendicular to the axis of the cantilever.

3 Results and discussion

3.1 Formation of films with congested morphology

The in-situ formation of ultrathin triboreactive ZDDP and DDP films is illustrated in Figure 2. The films were generated using the rubbing action between an AFM tip and a steel substrate in a liquid medium of PAO base oil containing ZDDP or DDP additive, as demonstrated in Figure 2a. The congested morphology was achieved using 128, 64 and 32 scanning lines (Figure 2b) rubbing at high temperature and contact force, which make the films grow thicker and wider over sliding cycles as illustrated in Figure 2c. The large number of scanning lines results in a maximum spacing distance of 156 nm separating any two lines, which is comparable to the estimated diameter of the AFM tip, i.e. about 150 nm. Therefore, the formed triboreactive films (Figure 2d-g), appear to have a continuous structure without any apparent distinctive lines.

In the case of ZDDP, two features appear in its triboreactive films (Figure 2d-f) during the early sliding cycles, i.e. < 3000 cycles. The first feature is the distinctive arranged pads that are formed initially under the scanning lines of the tip. As rubbing continued, the size of the pads increased until they became less uniform. For instance, a comparison between the formed films using 128 lines (Figure 2d) after 800 and 2000 cycles confirms this observation.

The second interesting feature observed during the first 3000 cycles of the film's formation is the accumulated film formed near the edges, which has larger thickness, i.e. nearly twice, than the one away from the edges. The reason behind this enlarged thickness can be related to several reasons. First, the change in the sliding velocity profile near the edges as the AFM tip changes direction can accelerate the rate of the tribochemical reaction of the ZDDP decomposition to form more zinc phosphate layers by lowering the reaction's time-dependent energy barrier[35]. Second, the larger number of sliding cycles experienced near the edges due to the narrower gap between the adjacent raster scanning lines (Figure 2b) can enhance the formation rate. Third, the flowability of the film as the AFM tip rasters the surface can push the film's pads to the sides. This is supported by the continuous increase in the area of the formed films, whether ZDDP (Figure 2h-j) or DDP (Figure 2k), over sliding cycles.

The areas of small thickness away from the edges appear to increase in thickness until they match the ones near the edges. This is counterintuitive to what is generally expected to be a uniform and continuous increase in thickness throughout the film as long as the initial conditions are maintained. The inconsistent growth might originate from the intrinsic limiting thickness of the thick regions of the film as they can be deformed easily leading to larger contact area and thus results in lower contact pressure and consequently low formation rate[15]. Another explanation can be related to what appears as removal cycles following the initial formation cycles once the film reaches a certain thickness (Figure 2h-i). These appear to be induced by the progressive shearing of the interface causing the weakly adhered top layers of the film to be removed or reallocated within the central area of the evolving film. Following the changes in the formed films using 128 lines (Figure 2d and h) after 2600, 3000 and 4000 cycles, reveals that the formation and removal of the film occur as follows. First, the film reaches a certain limiting thickness.

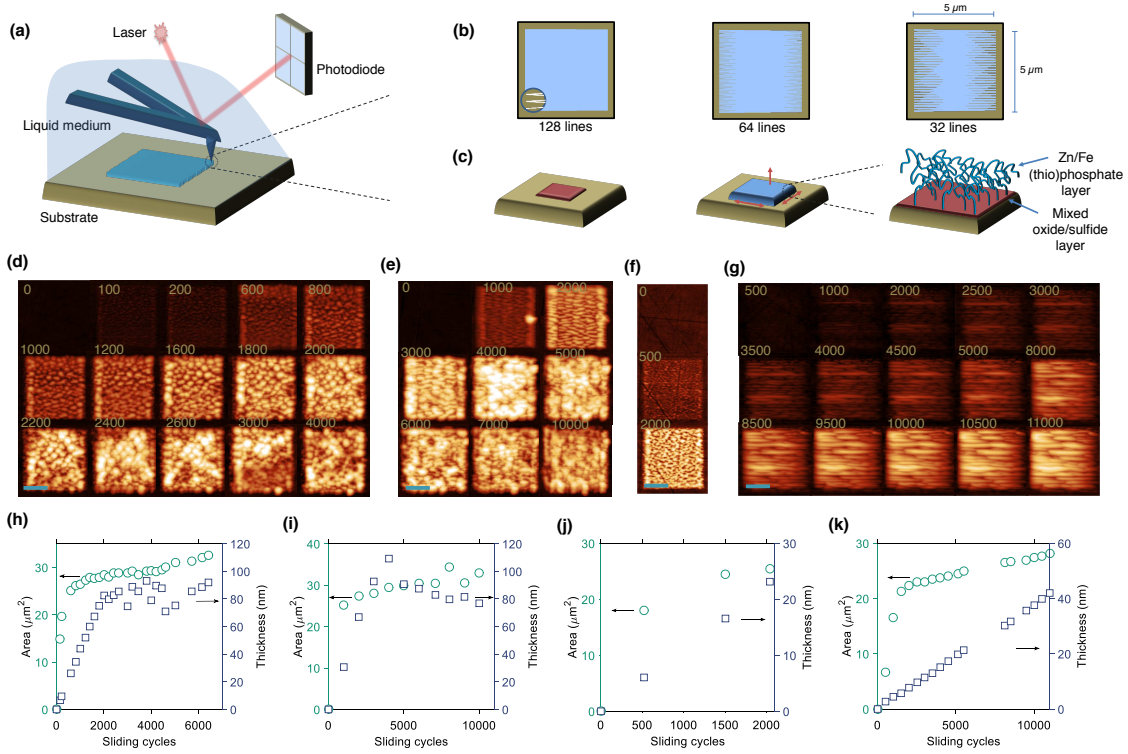

Figure 2. In-situ generation of ultrathin triboreactive ZDDP and DDP films using AFM. a, Schematic of the in-situ AFM liquid cell. b, Representation of the lines used to raster scanning a $5 \times 5\,\mu m^2$ area. c, Morphology evolution the formed films under rubbing at high temperature and applied force. d, e, and f, ZDDP films generated using 128, 64 and 32 lines, respectively, after different scanning cycles at 80 °C and 7.3 GPa. g, DDP films generated using 64 lines raster scanning at 80 °C and 4.8 GPa. h, i, and j, Analysis of thickness and area evolution over sliding cycles of the ZDDP reactive films formed using 128, 64 and 32 lines, respectively. k, The evolution of the area and thickness of the DDP films formed using 64 scanning lines. The scale bars on all the AFM images represent 2 μm.

Second, the thickest regions of the film start to be removed first followed by the neighbouring regions, as indicated in the drop in thickness after the 3000 cycle. Finally, a new cycle of formation starts, as indicated by the increase in film thickness after the 4000 cycle compared to its previously recorded state. These formation and removal cycles appear to be repetitive in nature.

The evolution of the DDP triboreactive films over sliding cycles formed using 64 scanning lines at 4.8 GPa (Figure 2g) appears to be different from that of ZDDP films. The DDP films do not appear to have larger thickness near the edges during the early stage of rubbing compared to the central region, but instead they appear to have a uniform morphology throughout with large pads elongated in the direction of shear. In addition, the DDP films appear to have non-uniform thickness that depends mainly on the initially formed regions, which keep growing more than the rest of the film. As rubbing cycles progressed, further shearing does not appear to cause severe mixing and distortion to the individual pads, which leads to the preservation of the initial structure of the triboreactive film despite the increase in thickness (Figure 2k). All these features are different from those observed previously in the case of the ZDDP films. The reason behind this can be related to the type of the phosphate composing the main bulk of the triboreactive film. In the case of the ZDDP films, predominantly zinc phosphate of relatively long chain length is formed[3,6,7,10,13] compared to iron phosphate of short chain length in the case of DDP films[36–38]. Thus, the type of cations available during the decomposition of the additive appears to not only affect the composition but also the structure and possibly the flowability behaviour of the formed film.

3.2 Formation of films with nanostructured morphology

The formation of ultrathin triboreactive ZDDP and DDP films with nanostructured morphology using the AFM is illustrated in Figure 3a. To explore the structural dynamics of the formed pads of the triboreactive films, few scanning lines, i.e. 16, 8, 4 and 1, were used (Figure 3b). At high temperature and contact force, the unrestrained pads formed on these lines can grow thicker and wider over sliding cycles (Figure 3c) as the maximum separation distance between any two adjacent lines is > 312 nm, which is much larger than the estimated diameter of the AFM tip. This is the reason behind the appearance of clear distinctive

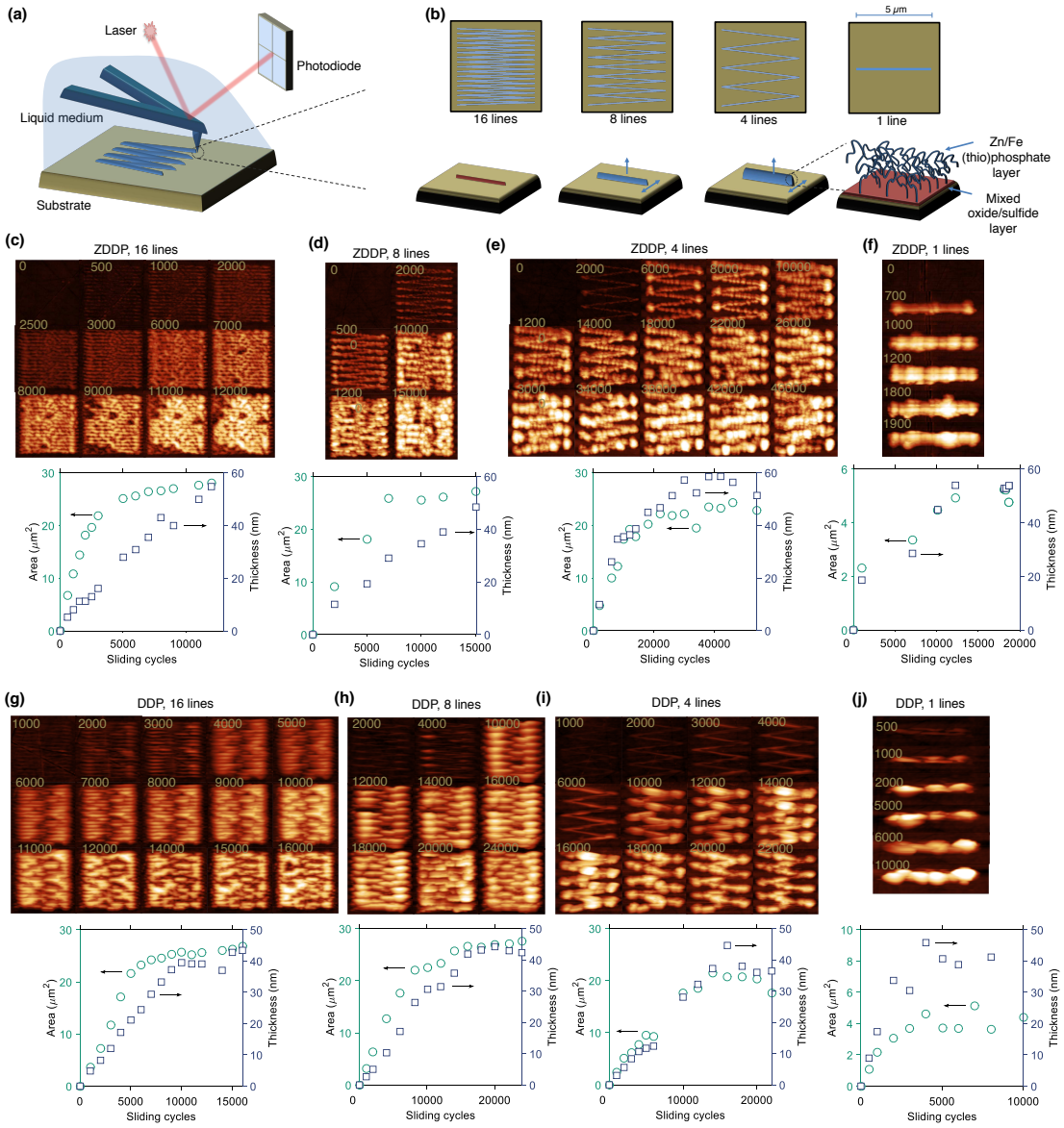

Figure 3. In-situ generation of ultrathin triboreactive ZDDP and DDP films using AFM. a, Schematic of the in-situ AFM liquid cell. b, Representation of the lines used to raster scanning a $5 \times 5\,\mu m^2$ area. c, Morphology evolution of the formed films under rubbing at high temperature and applied force. d-g, ZDDP films generated using 16, 8, 4 and 1 scanning lines, respectively, after different rubbing cycles at 80 °C and 7.3 GPa. h-k, DDP films generated using 16, 8, 4 and 1 scanning lines, respectively, after different rubbing cycles at 80 °C and 4.8 GPa. The analysis of thickness and area evolution of the reactive films over sliding cycles are shown under the AFM images. The scale bars on all the AFM images represent 2 μm.

lines during the early stages of the film formation whether in the case of ZDDP (Figure 3d-g) or DDP (Figure 3h-k).

Several common features appear in the case of the ZDDP films (Figure 3d-f), which are similar to those observed for larger numbers of scanning lines (Figure 2). The first feature is related to the thicker film formed near the edges compared to the middle areas, which can be related to different causes including the film flowability, change in tip velocity and double rubbing action at these regions as the scanning lines get closer to each other and finally overlap when moving towards the edges. The second feature is related to the uniform structure of the formed film during the early stages compared to the final stages, which can be attributed to the wear action and the intrinsic deterministic nature of the film formation. As rubbing continues, deviations and less uniform film are increasingly expected because of wear and smearing of the thick areas of the film under shear. This is evident from the worn areas near the edges where the film was initially thicker. Thus, the results indicate that the ZDDP triboreactive film exhibits a dynamic sacrificial nature allowing it to be continuously formed and removed[24].

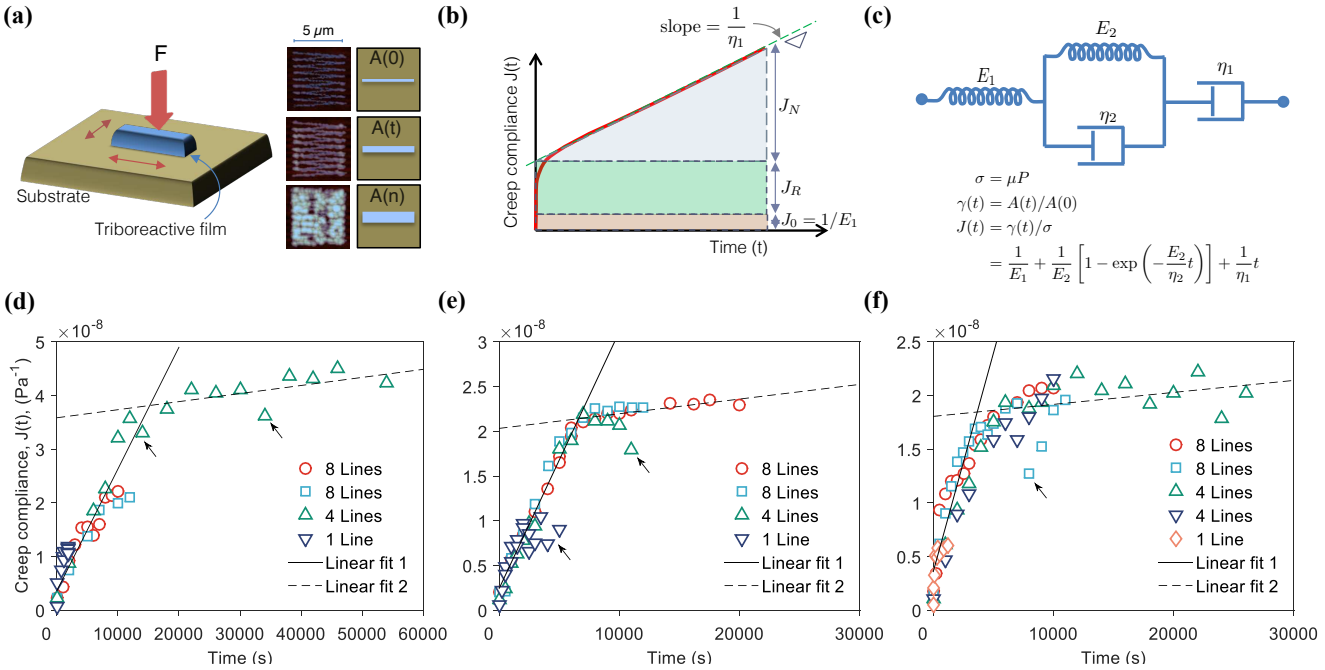

Figure 4. Viscosity quantification of triboreactive ZDDP films using creep method. a, Schematic representation of the creep-based method and sample of AFM masked images used to calculate the area evolution of the formed films. b, Illustration of a creep compliance curve during creep-recovery experiment. c, The Burgers material model used to fit the creep compliance data. d-f, Evolution of the creep compliance, $J(t)$, over time using different scanning lines, i.e. 8, 4 and 1 at 80 °C for (d) ZDDP films formed at 4.5 GPa and (e, and f,) DDP films formed at 4.8 and 5.6 GPa, respectively. Arrows indicate instances of film removal.

Another interesting feature is observed in the scanning lines that become less visible as the film grows. Two factors can cause this behaviour to occur. First, rubbing might have pushed the worn parts of the film into the areas between the scanning lines. Second, the film itself might be soft and deformable. Thus, it is plausible that the interfacial shear stress and large contact pressure caused the thick soft areas of the film to flow and consequently cover the gaps between the adjacent scanning lines. This can be confirmed for the case of ZDDP (Figure 3d-g) and DDP (Figure 3h-k) films by observing the increase in the thickness of the formed films and spreadability of their areas over sliding cycles even in the case of a single scanning line. Based on these observations, the structure of the triboreactive films appears to evolve as follows. Initially, the film is formed under the scanning lines where the interface between the steel surface and AFM tip experiences large shear stress and contact pressure. However, as shearing continues and film thickness increases, the film gradually starts to fill the nearby areas. The structure of the film appears as if it flows from the areas of high contact pressure to spread to any available gap.

The results suggest that contrary to the generally perceived conception that the P-based triboreactive films, such as the ones of ZDDP, are rigid[16,24,39], they appear to behave as a highly viscous material that can deform and flow under shear. The significant implication of this finding is that for the first time it provides a novel mechanistic understanding for the excellent antiwear properties of the ZDDP and DDP pads. In addition to forming a mechanical barrier, the film can also deform and flow. Thus, it mitigates the shear stress at the contacting asperities leading to less wear. A similar conclusion can also be inferred from the results of Pereira et al.[40] who showed that below 200 °C the modulus of the ZDDP film was nearly constant at around 100 GPa but dropped to about 70 GPa at 200 °C. The decrease in the modulus can indicate a compliant film that might be easily deformed. The results of Pereira et al.[40] were obtained by heating an already formed triboreactive film, whereas here we observe the film deformation in-situ during its formation at much lower temperature, which suggests that shear at high contact pressure can induce deformation even at low temperatures.

3.3 Viscosity quantification using creep

In the creep experiments, a fixed stress is applied and the resulting deformation is observed (Figures 4 and S8). The performed AFM experiments described in Figure 2 and 3 can be considered as creep experiments. In those experiments, the AFM tip applies a constant stress via contact pressure on a certain initial area of the formed film, which undergoes deformation and flowability in the lateral direction (Figure 4a). The shear stress σ can be estimated to be dependent on the friction coefficient μ

and contact pressure P, i.e. $\sigma = \mu P$, assuming the two are constant. The strain $\gamma(t)$ can be obtained by normalizing the area of the film $A(t)$ evolving over time by the initial film area $A(0)$ under the AFM tip, i.e. $\gamma(t) = A(t)/A(0)$. The creep compliance $J(t)$ can then be found by dividing the strain by the applied stress, i.e. $J(t) = \gamma(t)/\sigma$. In the limit of linear viscoelasticity, the creep compliance can be defined using a Burgers material model (Figure 4c), as follows:

$$J(t) = J_0 + J_R\psi(t) + \frac{1}{\eta_1}t \tag{1}$$

$$= \frac{1}{E_1} + \frac{1}{E_2}\left[1 - \exp\left(-\frac{E_2}{\eta_2}t\right)\right] + \frac{1}{\eta_1}t \tag{2}$$

where J_0 is the instantaneous creep compliance, J_R is the total recoverable compliance, and $\psi(t)$ is the delayed elasticity function, which is zero at time zero and one for $t \longrightarrow \infty$. As the ZDDP and DDP triboreactive films are formed of polyphosphate chains of relatively small polymerisation number $\lessapprox 10$[41], and considering the creep behaviour after long time during which the elastic contribution can be neglected and the creep compliance approaches a linear steady state, only the last term of Equation 1 (i.e. the viscous contribution) is of importance (Figure 4b-c).

The evolution of the creep compliance over time for different ZDDP and DDP films formed using different scanning lines, i.e. 8, 4 and 1, is shown in Figure 4d-f. In order to obtain these results several assumptions and considerations were taken into account. First, the flowability was considered to occur in the direction across the formed film as well as in the direction along the action of shear (Figures S8 and S9). Second, the film growth (formation and removal) and flowability were supposed to occur simultaneously, which were readily decoupled as the growth occurs only in the vertical direction whereas flowability in the lateral direction. In the case that a big removal event occurs such that the covered area with the film decreases, this is registered as a sharp drop in the followed film creep compliance, as identified by the arrows in Figure 4d-f. Third, the geometry of the tip-substrate counterbodies can be simplified to a plate-plate geometry without a direct contact between them but separated by the film. This is a rough oversimplification that can be especially applied for worn tips and for films of thickness larger than the substrate roughness, i.e. $>$ 13 nm. Fourth, in the limiting case of small gaps, viscosity is not affected by the shear rate but solely by the shear stress[42].

The compliance evolution over time (Figure 4d-f) indicates two creep regimes. Initially, the film experiences a primary fast linear creep as the neighbouring pads were not completely restrained followed by a secondary slower linear creep when the pads became congested. The Newtonian viscosity, i.e. the inverse slope of the compliance versus time as suggested by Equation 1, was estimated based on the two creep regimes. The primary creep suggests a viscosity of about $5-7\times10^{11}$ Pa.s as opposed to $7-9\times10^{12}$ Pa.s for the secondary regime. These results are comparable to the bulk viscosity of various metallic glasses near and above their glassy transition temperature, i.e. $T_g > 350$ °C, as reported in the literature using bulk rheometry[43–46]. The close viscosities between the P-based films of ZDDP and DDP and metallic glasses confirm that the final structure of the P-based films is merely a final solidified image of what once was hot, flowing and molten phosphate glass. For the first time, this evidences how rubbing can accelerate the formation of a highly viscous amorphous phosphate glass that helps protect contacting surfaces from excessive wear.

3.4 Viscosity quantification using squeeze-flow

Quantifying the viscosity using the squeeze flow analysis is based on squeezing the triboreactive film between two parallel plates, as depicted in Figure 5a, and observing the thickness evolution of the film over time. In our experiments, one of the plates is the AFM tip and the other is the steel substrate. To limit this effect to genuine flowability and avoid any formation, the experiments were carried out ex-situ at ambient temperature in base oil without any reactive additive after a continuous film was formed.

The results of ZDDP (Figure 5b) and DDP films (Figure 5c) show that when a small contact pressure was applied the film initially covered an area of $5\times5\,\mu m^2$. However, when the contact pressure was increased to 2.7 GPa and subsequently to 3.7 GPa, the covered area increased to about $6\times6\,\mu m^2$ and $7\times7\,\mu m^2$, respectively. Further increase of contact pressure to 4.5 GPa did not appear to have any significant effect on the film area, which can be a result of wear that reduces the area proportionally to the increase caused by the squeeze flow.

The removal amount can be readily quantified and decoupled from the true flowability by observing the changes in the area and volume of the ZDDP (Figure 5d) and DDP films (Figure 5f). In case of flow without wear, the volume of the squeezed film should be preserved as its area spreads and thickness decreases. However, in case of flow accompanied by wear, the volume can decrease because of removal of parts of the film. This reduction can be subtracted from the apparent film volume to obtain its evolution due to flowability only as shown in Figure 5b for the case of ZDDP and in Figure 5c for the case of DDP.

Counterintuitive to the expected decrease in the film thickness due to its flow or removal, a small recovery in the film volume was observed when the contact pressure was increased from 2.1 to 2.7 GPa. The source of this recovery might be

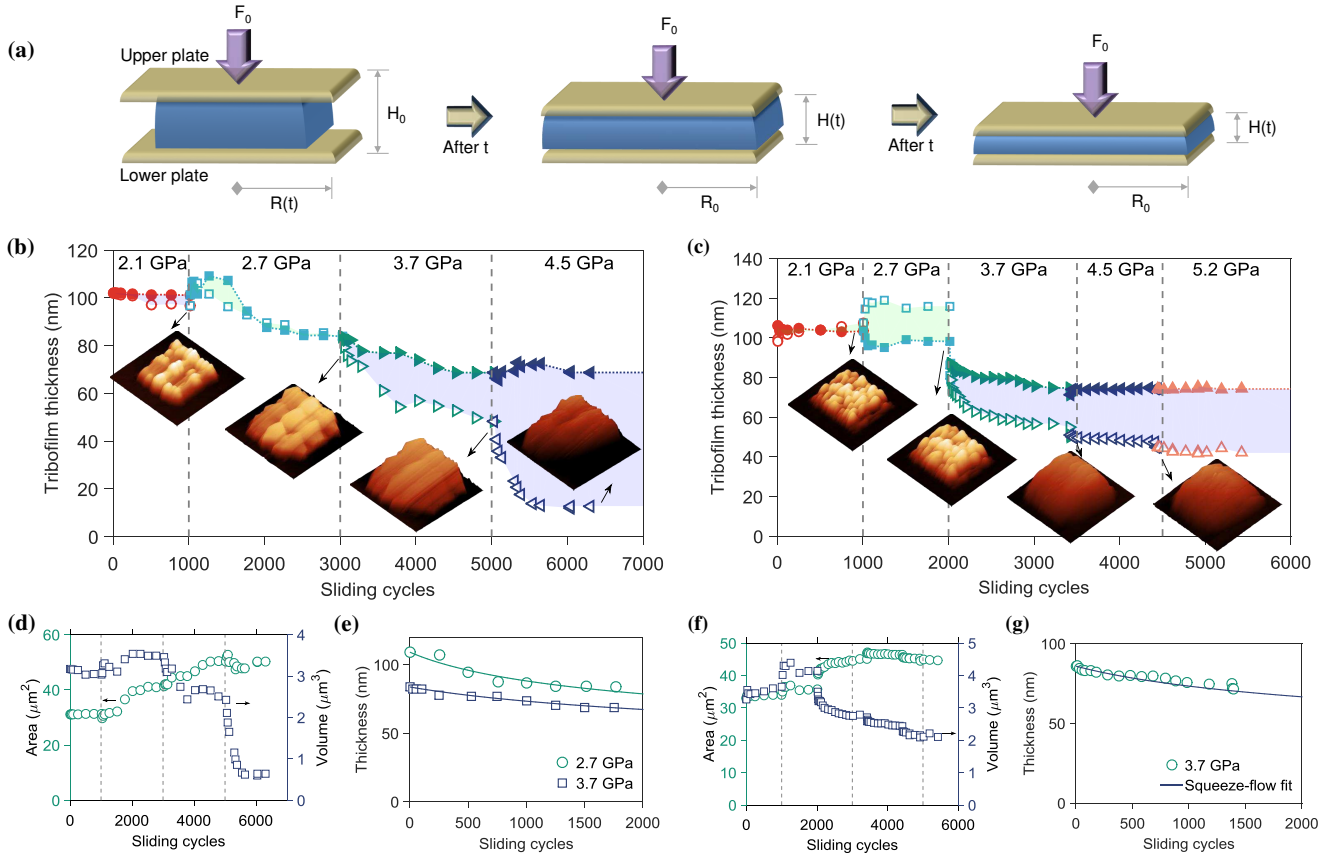

Figure 5. Viscosity quantification using squeeze-flow method of continuous ZDDP and DDP triboreactive films formed using 64 scanning lines. a, Schematic of the squeeze flow between two parallel plates assuming constant volume before and after applying a constant load over short and long squeeze times. b and c, Evolution of the total film thickness (open symbols) and film thickness without wear (closed symbols) for the case of ZDDP and DDP films, respectively, after different sliding cycles at 25 °C under different contact pressures. Green areas indicate increase in film thickness whereas blue areas indicate film removal. d and f, Analysis of the volume and area of the ZDDP and DDP films, respectively. e and g, Fits of the thickness of the ZDDP and DDP films, respectively, using Equation 3.

related to two possible causes. First, the high contact pressure can induce transformation in the entrapped adsorbed ZDDP molecules within the film or any remnant of alkyl phosphate on the film's surface[12] into phosphate with zinc or iron cation modifier in the case of ZDDP and DDP film, respectively. Second, the high contact pressure can cause irreversible disruption of the local compactness of the interfacial layers of the film leading to an increase in the free volume within the phosphate glass layers. This makes the film loose and more susceptible to wear, which is confirmed by the subsequent decrease in the film volume over the sliding cycles.

In the most simplified case, the flowability of the triboreactive films can be considered Newtonian. Therefore, the viscosity, μ, of the triboreactive films can be quantified by following the gap evolution $H(t)$, i.e. the film thickness, while it is squeezed as follows[47]:

$$H(t) = H_0 \left(1 + \frac{8H_0^2 F_0 t}{3\pi\mu R_0^4}\right)^{-1/4} \tag{3}$$

where H_0 is the initial film thickness just before applying load F_0, $H(t)$ is the film thickness over time and R_0 is the initial radius of the squeezed film, which can be taken as the tip radius. The experimental data discussed before in Figure 5 can be fitted using the above equation to obtain the film viscosity, which is the only unknown. The result of this fitting is shown in Figure 5e and g for ZDDP and DDP film, respectively, which shows that in average the Newtonian viscosity of the film is about $2-6\times10^{11}$ Pa.s. These are similar to the values obtained using the creep experiments. Similar values were also obtained

by applying the creep methodology to analyse the squeeze-flow data (Figures S11 and S12). In addition, viscosity values within one order of magnitude, i.e. from 2×10^{12} to 8×10^{13} Pa.s, with a similar flowability behaviour (Figures S13-S18) were obtained by simulating the elasto-plastic deformation of the ZDDP tribofilm. The different independent experimental methods, i.e. creep and squeeze flow, and modelling work suggest unambiguously that under rubbing the formed tribofilm of amorphous Zn/Fe phosphate behaves as a molten glass despite the relatively low temperature of the oil of 80 ^{o}C. This suggests that one of the antiwear mechanisms of the P-based additives is to form a highly viscous glass on the contacting surfaces that helps reduce wear and mitigate contact stresses.

3.5 Comparison between creep and squeeze-flow methods

The viscosity values based on either creep or squeeze flow experiments are close to the reported values in literature for ZDDP films, i.e. 10^8 Pa.s[12]. However, these values are two to three decades lower than the ones estimated in this study. Several factors might be responsible for this discrepancy. First, Bec et al.[12] did not actually measure the viscosity of the ultrathin P-based films, but instead they related it to the measured elastic modulus. Thus, it was more of a numerical estimation than an experimental quantification. Second, there is a significant difference between the experimental methods used in this study compared to the previous one. The current study implemented two novel methods using the AFM with a tip radius less than 80 nm, whereas the previous study of Bec et al.[12] used the surface-force apparatus with a sphere of radius of 2.125 mm. The large difference in the probe size indicates that the viscosity values reported in the previous studies were averaged over a large area of the film, whereas the current ones are of localized area within the film. As the film typically consists of ridges and troughs of heterogeneous mechanical properties as well as varied thickness and composition, it follows that the averaged properties measured by a large probe can be different from the local ones measured by a significantly smaller probe.

3.6 Conclusion

The textural and rheological properties of nano-thin P-based triboreactive films were followed over time to better understand the origin of their superior antiwear properties. The obtained results confirm that the films behave as a molten glass with an average viscosity of 1×10^{12} Pa.s. This suggests that their superior antiwear properties originate from their intrinsic rheological properties that allow them to flow while formed, which is clear from their ability to maintain local order on the nanoscale through the motion of the formed tribofilm's pads at the interface. This appears to effectively mitigate the smearing and wearing of the contacting asperities resulting in less wear. The findings of this study open future opportunities for quantitatively analysing the rheology of a broad range of additives and substrates and its relation to the tribological properties, which can help build mechanistic models capable of better predicting friction and wear, and thus optimise energy consumption. In addition, this study highlights the potential of using nano-flowable glasses to efficiently control the lubrication in tomorrow's engines without the need of using harmful oil additives.

4 Data availability

The datasets associated with the current study are available from the corresponding author on reasonable request.

5 Acknowledgements

This work is supported by EPSRC (grant number EP/R001766/1) and Marie Curie Initial Training Networks (grant number 317334).

6 Additional information

Competing financial interests (The authors declare no competing interests).

References

1. Holmberg, K., Andersson, P. & Erdemir, A. Global energy consumption due to friction in passenger cars. *Tribol. Int.* **47**, 221–234 (2012).
2. Holmberg, K. & Erdemir, A. Influence of tribology on global energy consumption, costs and emissions. *Friction* **5**, 263–284 (2017).
3. Spikes, H. The History and Mechanisms of ZDDP. *Tribol. Lett.* **17**, 469–489 (2004).
4. Nicholls, M. a., Do, T., Norton, P. R., Kasrai, M. & Bancroft, G. Review of the lubrication of metallic surfaces by zinc dialkyl-dithiophosphates. *Tribol. Int.* **38**, 15–39 (2005).

5. Jones, R. & Coy, R. The chemistry of the thermal degradation of zinc dialkyldithiophosphate additives. *Asle Transactions* **24**, 91–97 (1981).

6. Dorgham, A., Neville, A. & Morina, A. Tribochemistry and morphology of p-based antiwear films. In *Advanced Analytical Methods in Tribology*, 159–214 (Springer, 2018).

7. Dorgham, A., Parsaeian, P., Neville, A., Ignatyev, K., Mosselmans, F., Masuko, M. & Morina, A. In situ synchrotron xas study of the decomposition kinetics of zddp triboreactive interfaces. *RSC Adv.* **8**, 34168–34181 (2018).

8. Fuller, M. L. S., Kasrai, M., Bancroft, G. M., Fyfe, K. & Tan, K. H. Solution decomposition of zinc dialkyl dithiophosphate and its effect on antiwear and thermal film formation studied by x-ray absorption spectroscopy. *Tribol. international* **31**, 627–644 (1998).

9. Bell, J., Delargy, K. & Seeney, A. Paper ix (ii) the removal of substrate material through thick zinc dithiophosphate anti-wear films. *Tribol. series* **21**, 387–396 (1992).

10. Dorgham, A., Neville, A., Ignatyev, K., Mosselmans, F. & Morina, A. An in situ synchrotron xas methodology for surface analysis under high temperature, pressure, and shear. *Rev. Sci. Instruments* **88**, 015101 (2017).

11. Baldwin, B. Wear mitigation by antiwear additives in simulated valve train wear. *Asle Transactions* **26**, 37–47 (1983).

12. Bec, S., Tonck, A., Georges, J.-M., Coy, R., Bell, J. & Roper, G. Relationship between mechanical properties and structures of zinc dithiophosphate anti–wear films. In *Proceedings of the Royal Society of London A: Mathematical, Physical and Engineering Sciences*, vol. 455, 4181–4203 (The Royal Society, 1999).

13. Dorgham, A., Azam, A., Morina, A. & Neville, A. On the transient decomposition and reaction kinetics of zinc dialkyldithiophosphate. *ACS applied materials & interfaces* **10**, 44803–44814 (2018).

14. Dorgham, A. *Reaction kinetics and rheological characteristics of ultra-thin P-based triboreactive films*. Ph.D. thesis, University of Leeds (2018).

15. Gosvami, N., Bares, J., Mangolini, F., Konicek, A., Yablon, D. & Carpick, R. Mechanisms of antiwear tribofilm growth revealed in situ by single-asperity sliding contacts. *Science* **348**, 102–106 (2015).

16. Nicholls, M. a., Norton, P. R., Bancroft, G. M., Kasrai, M., Stasio, G. D. & Wiese, L. M. Spatially resolved nanoscale chemical and mechanical characterization of ZDDP antiwear films on aluminum–silicon alloys under cylinder/bore wear conditions. *Tribol. Lett.* **18**, 261–278 (2005).

17. Martin, J. M. Antiwear mechanisms of zinc dithiophosphate: a chemical hardness approach. *Tribol. letters* **6**, 1–8 (1999).

18. Martin, J. M., Grossiord, C., Le Mogne, T., Bec, S. & Tonck, A. The two-layer structure of zndtp tribofilms: Part i: Aes, xps and xanes analyses. *Tribol. international* **34**, 523–530 (2001).

19. Pidduck, A. & Smith, G. Scanning probe microscopy of automotive anti-wear films. *Wear* **212**, 254–264 (1997).

20. Bird, R. & Galvin, G. The application of photoelectron spectroscopy to the study of ep films on lubricated surfaces. *Wear* **37**, 143–167 (1976).

21. Dorgham, A., Wang, C., Morina, A. & Neville, A. 3d tribo-nanoprinting using triboreactive materials. *Nanotechnology* **30**, 095302 (2019).

22. Friedenberg, M. C. & Mate, C. M. Dynamic viscoelastic properties of liquid polymer films studied by atomic force microscopy. *Langmuir* **12**, 6138–6142 (1996).

23. Warren, O., Graham, J., Norton, P., Houston, J. & Michalske, T. Nanomechanical properties of films derived from zinc dialkyldithiophosphate. *Tribol. Lett.* **4**, 189–198 (1998).

24. Aktary, M., McDermott, M. & McAlpine, G. Morphology and nanomechanical properties of ZDDP antiwear films as a function of tribological contact time. *Tribol. letters* **12**, 155–162 (2002).

25. Ye, J., Araki, S., Kano, M. & Yasuda, Y. Nanometer-scale Mechanical/Structural Properties of Molybdenum Dithiocarbamate and Zinc Dialkylsithiophosphate Tribofilms and Friction Reduction Mechanism. *Jpn. J. Appl. Phys.* **44**, 5358–5361 (2005).

26. Glor, E. C. & Fakhraai, Z. Facilitation of interfacial dynamics in entangled polymer films. *The J. chemical physics* **141**, 194505 (2014).

27. Daley, C., Fakhraai, Z., Ediger, M. & Forrest, J. Comparing surface and bulk flow of a molecular glass former. *Soft Matter* **8**, 2206–2212 (2012).

28. Thomas, K. R., Chenneviere, A., Reiter, G. & Steiner, U. Nonequilibrium behavior of thin polymer films. *Phys. Rev. E* **83**, 021804 (2011).

29. Qi, D., Ilton, M. & Forrest, J. Measuring surface and bulk relaxation in glassy polymers. *The Eur. Phys. J. E: Soft Matter Biol. Phys.* **34**, 1–7 (2011).

30. Fakhraai, Z. & Forrest, J. Measuring the surface dynamics of glassy polymers. *Science* **319**, 600–604 (2008).

31. Bodiguel, H. & Fretigny, C. Reduced viscosity in thin polymer films. *Phys. review letters* **97**, 266105 (2006).

32. Bodiguel, H. & Frétigny, C. Viscoelastic dewetting of a polymer film on a liquid substrate. *The Eur. Phys. J. E: Soft Matter Biol. Phys.* **19**, 185–193 (2006).

33. Fakhraai, Z. & Forrest, J. A. Probing slow dynamics in supported thin polymer films. *Phys. review letters* **95**, 025701 (2005).

34. Liu, J., Notbohm, J. K., Carpick, R. W. & Turner, K. T. Method for characterizing nanoscale wear of atomic force microscope tips. *ACS nano* **4**, 3763–3772 (2010).

35. Tysoe, W. On stress-induced tribochemical reaction rates. *Tribol. Lett.* **65**, 48 (2017).

36. Najman, M., Kasrai, M. & Bancroft, G. Chemistry of antiwear films from ashless thiophosphate oil additives. *Tribol. Lett.* **17**, 217–229 (2004).

37. Kim, B., Sharma, V. & Aswath, P. B. Chemical and mechanistic interpretation of thermal films formed by dithiophosphates using xanes. *Tribol. Int.* **114**, 15–26 (2017).

38. Zhang, Z., Yamaguchi, E., Kasrai, M., Bancroft, G., Liu, X. & Fleet, M. Tribofilms generated from zddp and ddp on steel surfaces: Part 2, chemistry. *Tribol. Lett.* **19**, 221–229 (2005).

39. Ye, J., Kano, M. & Yasuda, Y. Friction property study of the surface of zddp and modtc antiwear additive films using afm/lfm and force curve methods. *Tribotest* **9**, 13–21 (2002).

40. Pereira, G., Munoz-Paniagua, D., Lachenwitzer, A., Kasrai, M., Norton, P. R., Capehart, T. W., Perry, T. A. & Cheng, Y.-T. A variable temperature mechanical analysis of zddp-derived antiwear films formed on 52100 steel. *Wear* **262**, 461–470 (2007).

41. Crobu, M., Rossi, A., Mangolini, F. & Spencer, N. D. Chain-length-identification strategy in zinc polyphosphate glasses by means of xps and tof-sims. *Anal. bioanalytical chemistry* **403**, 1415–1432 (2012).

42. Clasen, C., Kavehpour, H. P. & McKinley, G. H. Bridging tribology and microrheology of thin films. *Appl. Rheol* **20**, 196 (2010).

43. Johnson, W. L. Bulk glass-forming metallic alloys: Science and technology. *MRS bulletin* **24**, 42–56 (1999).

44. Wang, W.-H., Dong, C. & Shek, C. Bulk metallic glasses. *Mater. Sci. Eng. R: Reports* **44**, 45–89 (2004).

45. Waniuk, T., Busch, R., Masuhr, A. & Johnson, W. Equilibrium viscosity of the zr 41.2 ti 13.8 cu 12.5 ni 10 be 22.5 bulk metallic glass-forming liquid and viscous flow during relaxation, phase separation, and primary crystallization. *Acta Materialia* **46**, 5229–5236 (1998).

46. Busch, R., Bakke, E. & Johnson, W. Viscosity of the supercooled liquid and relaxation at the glass transition of the zr 46.75 ti 8.25 cu 7.5 ni 10 be 27.5 bulk metallic glass forming alloy. *Acta Materialia* **46**, 4725–4732 (1998).

47. Engmann, J., Servais, C. & Burbidge, A. S. Squeeze flow theory and applications to rheometry: a review. *J. non-newtonian fluid mechanics* **132**, 1–27 (2005).